Behavior of Linear Beam-Plasma Instabilities in the Presence of Finite Amplitude Circularly Polarized Waves

L. Gomberoff,

Depto. de Física, Facultad de Ciencias, Universidad de Chile, Casilla 653, Santiago, Chile. (lgombero@uchile.cl)

J. Hoyos,

Depto. de Física, Facultad de Ciencias, Universidad de Chile, Casilla 653, Santiago, Chile. (jhoyos@fisica.ciencias.uchile.cl)

and A. L. Brinca

Centro de Física de Plasmas, Instituto Superior Técnico, 1049-001 Lisboa, Portugal. (ebrinca@alfa.ist.utl.pt)

Received on 11 December, 2004; revised version received on 22 April, 2004

We review the effect of finite amplitude circularly polarized waves on the behavior of linear ion-beam plasma instabilities. It has been shown that left-hand polarized waves can stabilize linear right-handed instabilities [1]. It has also been shown that for beam velocities capable of destabilizing left-handed waves, left-hand polarized large amplitude waves can also stabilize these waves. On the other hand, when the large amplitude wave is right-hand polarized, they can either stabilize or destabilize right-handed instabilities depending on the wave frequency and beam speed [2]. Finally, we show that the presence of large amplitude left-hand polarized waves can also trigger electrostatic ion-acoustic instabilities by forcing the phase velocities of two ion acoutic waves to become equal, above a threshold amplitude value.

1 Introduction

The nonlinear stability of finite amplitude circularly polarized electromagnetic waves in ion beam-plasma systems has been thoroughly studied through the years [3, 4] because of its importance in several space plasma environments and laboratory plasmas [3, 4, 5, 6, 7, 8]. Parametric wave-wave interactions of circularly polarized electromagnetic waves in a plasma involving alpha particles drifting relative to the proton, have been studied by [9, 10, 11]. Their nonlinear evolution has also been studied by using drift kinetic effects [12] and hybrid computer simulation techniques[13]. Studies have been carried out by [14, 15, 16], including the effects of dissipation and of the beam drift speed. The effect and the evolution of the beam for right and left handed polarized waves, have also been studied by using simulation experiments [17]. These studies have considered linearly stable systems[9, 10, 14, 15, 16]. Proton beams observed in the solar wind display large drift velocities which can be larger than the necessary velocity to generate a linear beam-plasma instability [18]. In [1], it was found that the behavior of linear electromagnetic right-handed polarized instabilities (r-instabilities) in a beam-plasma system can be affected by the presence of a finite amplitude left-handed polarized wave (L-wave). It was also shown that r-instabilities can be stabilized by L-waves in a linearly unstable proton beam-plasma system. These results were confirmed by using computer simulations [19], where it was also argued that the observational results of [18] could be explained by the presence of a large amplitude L-wave.

We also show here that the presence of an L-wave triggers electrostatic instabilities above a threshold amplitude. These instabilities occurs when the phase velocities of two sound waves are equal [9, 10, 20]. These authors have shown that when the ion acoustic wave phase velocity of the sound waves moving forward relative to the proton background and backward in the frame of the alpha particle become equal, they trigger electrostatic instabilities between these two modes. They also notice that the presence of a large amplitude L-wave can partially stabilize the electrostatic instability [9, 10, 20]. Here we show that even if initially the ion-acoustic waves moving forward and backward relative to the background proton core are stable, the presence of a large amplitude L-wave can force the phase velocities to become equal, triggering thereby, the electrostatic instability. In this sense the presence of the large amplitude wave can also affect the properties of the linear electrostatic streaming acoustic waves for an L-wave amplitude above a threshold value.

The plan of the paper is as follows. In Section 2, we briefly discuss the linear proton beam-plasma dispersion relation in the cold plasma approximation, and a brief derivation of the nonlinear dispersion relation for L and R-waves (finite amplitude right-hand polarized waves) will be presented. Next in Section 3, the nonlinear dispersion relation will be studied graphically for several situations. It is shown there that the threshold amplitude of L-waves required to stabilize the linear r-instabilities increases with increasing

proton-beam velocity and, for fixed drift velocity, it decreases with increasing L-wave frequency. For larger beam drift speeds, L-waves can also stabilize the left-hand polarized instability (l-instability). The mechanism is more efficient for L-wave frequencies closer to the proton gyrofrequency. In the case when there is a R-wave in the system, it is shown that the part of the linear unstable spectrum below the wave frequency (which, depending on the beam drift velocity, may involve right as well as left-handed instabilities) can be completely stabilized for pump wave amplitudes above a threshold value. It is also shown that the presence of R-waves produce the same stabilization effect on the linear r-instabilities. We have also found that the presence of a L-wave produces electrostatic instabilities above a threshold amplitude. These instabilities occur when the phase velocities of the forward and backward ion-acoustic sound waves supported by the background proton population become equal. The results are summarized and discussed in Section 4.

2 Dispersion Relation

The linear plasma dispersion relation for circularly polarized electromagnetic waves propagating in the direction of an external magnetic field in a system consisting of electrons, a proton core, and a proton beam, is given by [21, 22, 23, 24],

$$y_0^2 = \frac{x_0^2}{1-x_0} + \frac{\eta(x_0 - y_0 U)^2}{1-(x_0 - y_0 U)}, \qquad (1)$$

where $x_0 = \omega_0/\Omega_p$, $y_0 = k_0 v_A/\Omega_p$, $v_A = B_0/(4\pi n_p M_p)^{1/2}$ is the Alfvén speed, $U = V/v_A$ is the normalized beam velocity, $\eta = n_b/n_c$ is the beam density relative to the core density, $\Omega_p = qB_0/cM_p$ is the proton gyrofrequency.

The dispersion relation, Eq. (1), is valid in a current-free plasma and in the reference frame where the proton core is at rest [22]. For an alpha particle beam the dispersion relation was first derived by using kinetic theory in the semi-cold approximation [22], and later on by using fluid theory [9]. The dispersion relation for an arbitrary ion beam can be found in [21].

We now derive very briefly the nonlinear dispersion relation. To this end we use a fluid description of the plasma. We assume the plasma to be composed by electrons, background protons, proton beam, and an L-wave propagating along the external background magnetic field. Each plasma component satisfies the following fluid equation of motion,

$$\left(\frac{\partial}{\partial t} + \vec{u}\cdot\vec{\nabla}\right)\vec{u} = \frac{q_l}{m_l}\left(\vec{E} + \frac{1}{c}\vec{u}\times\vec{B}\right) - \frac{\vec{\nabla}p}{n_l m_l}, \qquad (2)$$

where $\vec{u}$ is the bulk velocity, q_l the electric charge, m_l the mass, $\vec{E}$ and $\vec{B}$ the electric and magnetic field respectively, and p the pressure.

As pointed out before, the dispersion relation given by Eq. (1) was first derived by linearizing Vlasov's equation [22], and using the semi-cold approximation. Later on, it was derived by using first order perturbation theory on the fluid Eqs. (2) for zero temperature[9]. Finally, it was also shown to be an exact solution of Eqs. (2) for zero pressure[11].

In order to derive the nonlinear dispersion relation, we follow a similar procedure to [9, 11]. Thus, we perturb the fluid Eqs. (2) including the left-hand polarized electromagnetic wave moving in the direction of the external magnetic field along the x-axis, as follows,

$$\begin{aligned} \delta u_x &= Re[u\exp(ikx - i\omega t)], \\ \delta E_x &= Re[\epsilon exp(ikx - i\omega t)], \\ \delta n_p &= n_0 Re[\frac{uk}{\omega - kV_{0x}}\exp(ikx - i\omega t)], \end{aligned} \qquad (3)$$

where $V_{0x} = V$ is the beam speed.

For quantities perpendicular to the external magnetic field we write,

$$\begin{aligned} \delta u_\perp &= u_+\exp(ik_+x - i\omega_+ t) + u_-\exp(ik_-x - i\omega_- t), \\ \delta B_\perp &= b_+\exp(ik_+x - i\omega_+ t) + b_-\exp(ik_-x - i\omega_- t), \\ \delta j_\perp &= j_+\exp(ik_+x - i\omega_+ t) + j_-\exp(ik_-x - i\omega_- t), \end{aligned} \qquad (4)$$

where $u_\perp = u_y + iu_z$, and similarly for $B_\perp$ and $j_\perp$. On the other hand, $k_\pm = k_0 \pm k$ and $\omega_\pm = \omega_0 \pm \omega$, where k_0 and ω_0 are the frequency and wavenumber of the pump wave, which satisfies the dispersion relation in Fig. 1.

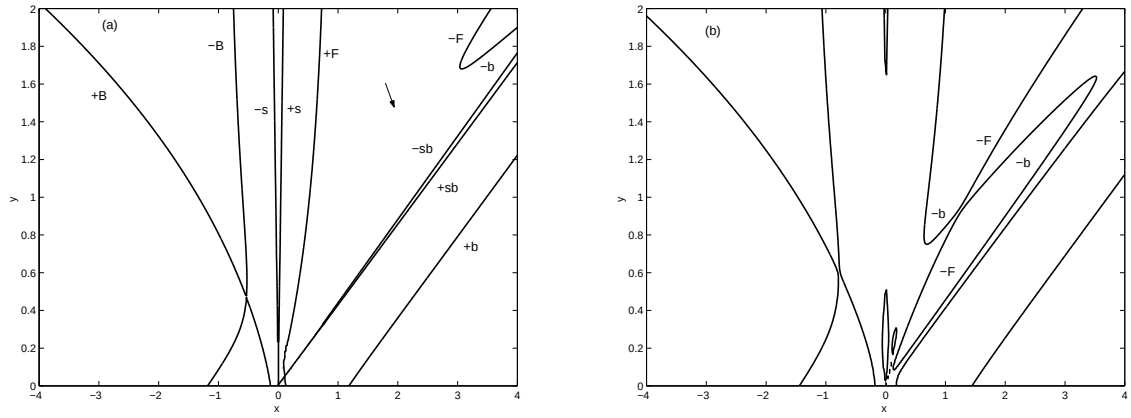

Figure 1. Nonlinear dispersion relation, Eq. (5), x vs. y, for $\eta = 0.2$, $U = 2.3$, $\beta_i = 0.001$, $x_0 = 0.1$, for (a) $A = 0$, and (b) $A = 0.81$.

$$L_+L_-D + L_+R_-B_{-cc} + L_+R_{-b}B_{-ccb} + L_-R_+B_+ + L_-R_{+b}B_{+b} + (B_{-cc}B_{+b} - B_{-ccb}B_+)(R_-R_{+b} - R_{-b}R_+)/D = 0. \quad (5)$$

In the last equation,

$$\begin{aligned}
L_\pm &= y_\pm^2 - x_\pm^2/\psi_\pm - \eta x_{\pm b}^2/\psi_{\pm b} \\
R_\pm &= y_\pm(x_0 - \frac{yx_0^2}{y_0x} + \frac{x_\pm}{\psi_\pm})/2\psi_0 \\
R_{\pm b} &= \eta y_\pm(x_{0b} - \frac{yx_{0b}^2}{y_0x_b} + \frac{x_{\pm b}}{\psi_{\pm b}})/2\psi_{0b} \\
D &= \beta_e'\Delta\eta r_b x^2 + \beta_e'\Delta_b r x_b^2 - \Delta\Delta_b(xx_b)^2 \\
B_+ &= -\beta_e'B_{+b1}\eta r x x_b + B_{+1}x^2(\beta_e'\eta r_b - \Delta_b x_b^2) \\
B_{+b} &= -\beta_e'B_{+1}r_b x x_b + B_{+b1}x_b^2(\beta_e' r - \Delta x^2) \\
B_{-cc} &= -\beta_e'B_{-ccb1}\eta r x x_b + B_{-cc1}x^2(\beta_e'\eta r_b - \Delta_b x_b^2) \\
B_{-ccb} &= -\beta_e'B_{-cc1}r_b x x_b + B_{-ccb1}x_b^2(\beta_e' r - \Delta x^2) \\
B_{+(b)1} &= -\frac{A\psi_{-(b)}(y_+\psi_{+(b)}x_{0(b)}^2 - y_0\psi_{0(b)}x_{+(b)}^2)}{y_0y_+x_{(b)}} \\
B_{-cc(b)1} &= \frac{A\psi_{+(b)}(y_-\psi_{-(b)}x_{0(b)}^2 - y_0\psi_{0(b)}x_{-(b)}^2)}{y_0y_-x_{(b)}} \\
\Delta &= A + r(1 - \frac{\beta_p y^2}{x^2}) \\
\Delta_b &= A + r_b(1 - \frac{\beta_b y^2}{x_b^2}) \\
\beta_l &= 4\pi n_p\gamma KT_l/B_0^2 \quad (l = e, c, b)
\end{aligned}$$

$$\begin{aligned}
x_b &= x - yU \\
x_{0b} &= x_0 - y_0U \\
A &= (\frac{B}{B_0})^2 \\
r_{(b)} &= \psi_{0(b)}\psi_{+(b)}\psi_{-(b)} \\
\psi_0 &= 1 - x_0 \\
\psi_{0b} &= 1 - x_{0b} \\
\psi_\pm &= 1 - x_\pm \\
\psi_{\pm b} &= 1 - x_{\pm b} \\
x_\pm &= x_0 \pm x \\
y_\pm &= y_0 \pm y \\
x_{\pm b} &= x_\pm - y_\pm U \\
\beta_e' &= \beta_e y^2/(1+\eta).
\end{aligned}$$

TABLE 1. Characterization of the various modes appearing in Eq. (5). The + (-) sign refers to the upper (lower) sideband waves, and lh (rh)left-hand (right-hand) polarization. F refers to the branch of the pump wave, and b to the branch due to the beam.

+ (-)	F	lh (rh) forward propagating
+ (-)	B	rh (lh) backward propagating
+ (-)	b	lh (rh) forward propagating
+ (-)	s	ion-acoustic forward (backward) propagation
+ (-)	sb	beam ion-acoustic forward (backward) propagation

The finite amplitude wave is characterized by the coordinates x_0 and y_0, and it is at the origin of the (x, y) coordinate system. For zero pump intensity, $A = 0$, Eq. (5) reduces to $L_+L_-D = 0$. The solution $L_\pm = 0$, corresponds to the dispersion relation of the upper and lower side band waves, respectively. The other solution $D = 0$, corresponds to the sound waves present in the system which, for $\eta \ll 1$, are given by,

$$x \simeq \pm(\beta_e + \beta_p)^{1/2}y, \quad (6)$$

$$(x - yU) \simeq \pm(\beta_b)^{1/2}y, \quad (7)$$

Eq. (6) corresponds to the ordinary ion-acoustic waves propagating forward and backward relative to the proton core in the directon of the magnetic field, and Eq. (7) corresponds to ion-acoustic waves supported mainly by the proton beam. They move forward and backward relative to the beam, along the external magnetic field. The solutions of $L_\pm = 0$ give the various branches of the dispersion relation. The crossings between the solutions give the position and nature of the possible wave couplings of the system. The solutions of the nonlinear dispersion relation, Eq. (5), are invariant under a rotation through an angle of 180^o. Therefore, it is sufficient to analyze the solutions in the upper half $\omega - k$ plane [9, 10, 20, 14, 15, 16]. Note that for $A = 0$, only the ion-acoustic modes depend on the temperature. Note also that the cold plasma dispersion relation for electromagnetic modes is a good approximation

in those regions of space where $\beta_{\|i} = (v_{th.\|i}/v_A)^2 \ll 1$ ($v_{th.\|i} = \sqrt{2KT_\| i/M_i}$) is the thermal velocity of species i). This may happen either for small temperatures -and also for not so small temperatures[27, 21]- or for very large Alfvén velocity relative to the thermal velocity, like e.g., in coronal holes [28, 29]. Eq. (5) corresponds to the dispersion relation for L-waves. The dispersion relation for R-waves can be obtained by replacing (x, y) by (-x, -y) and (x_0, y_0) by $(-x_0, -y_0)$. Alternatively, one can simply take $(-x_0, -y_0)$ for the frequency and wavenumber of the R-wave and leave the rest unchanged. This is so because the (x, y) plane is invariant under rotations through an angle of 180^o.

3 Graphical Analysis of the Nonlinear Dispersion Relation

In order to study the nonlinear dispersion relation Eq. (5) we use a graphical method first used by [30].

3.1 Linear Instabilities in the presence of L-waves

We start by studying the effect of varying proton-beam velocity on the stabilization of the linear r-instability due to the presence of an L-wave. In [1] it was shown that for $\beta_i = 0.001$, $\eta = 0.2$, $U = 2$, an L-wave of frequency $x_0 = 0.1$ stabilizes the linear r-instability for $A = 0.16$. As U increases, A_t is expected to increase too. In Fig. 1a we illustrate the situation for $U = 2.3$ and $A = 0$. The gap between the two curves denoted by -F and -b corresponds to the linear r-instability [1]. The lines denoted by -F and -b are lower R sideband waves propagating in the direction of the external magnetic field [1]. In Fig. 1b, $A = 0.81$ and the gap between -F and -b has disappeared showing, thereby, complete stabilization of the linear r-instability. Thus, the threshold amplitude is now $A_t = 0.81$, instead of $A_t = 0.16$ for $U = 2$ as expected, A_t increases with increasing U [1]. In Fig. 2a we have taken $x_0 = 0.5$, and $A = 0$. The other parameters are the same as in the previous figure. In Fig. 2b, we have taken $A_t = 0.7$, and the instability is completely stabilized. Thus, as the L-wave frequency increases, the threshold A_t-value decreases [1]. In general, for fixed U, the instability threshold continues to decrease as the L-wave frequency approaches the proton gyrofrequency. The effect is very pronounced for frequencies very close to the resonance. For example, for $U = 3$, and $x_0 = 0.3$, $A_t = 2.5$. However, for the same drift velocity but for $x_0 = 0.95$, $A_t = 0.47$. Finally, in Fig. 3 we consider the case $U = 2.8$. In this case there are both r and l-instabilities. In Fig. 3a we have plotted the nonlinear dispersion relation for $x_0 = 0.9$, and $A = 0$. The arrow shows the linear instability region. In Fig. 3b, $A = 0.63$. The linear instability is completely stabilized. including the l-instability region corresponding to Alfvén waves. It is simple to show that the l-instability is the first to be stabilized as A increases.

3.2 Linear Instabilities in the presence of R-waves

We shall now study the effect of an R-wave on the linear instability. To do this, as explained above, one can simply choose x_0 to be negative and leave the rest unchanged. Thus, we take an R-wave of frequency $x_0 = -0.1$. The other parameters are the same as in Fig. 1. In Fig. 4a we illustrate the linear instability for $A = 0$ and $U = 2$. This corresponds to the gap involving -F and -b. Note that these two roots correspond now to upper sideband waves while for an L-wave they correspond to lower sideband waves [1]. In Fig. 4b, A_t has been raised to $A = 0.146$. The gap has disappeared altogether indicating complete stabilization of the linear r-instability. This is a similar situation to [1], but now the stabilization is due to the presence of an R-wave. We shall now increase the beam drift velocity to $U = 4$. As shown in Fig. 5a, there are several linear instability regions, r/l-instabilities. The region between B and C, and D and O are r-instabilities, while the region between O and G is l-instability. In the following we study the effect of a R-wave on these instability regions. To this end, we take $x_0 = -0.1025$, with corresponding $y_0 = -0.1$. As it follows from Fig. 5a, in this case the pump wave is unstable. In Fig. 5b we show the nonlinear dispersion relation, Eq. (5), for $A = 0$. The other parameters are like in the previous figures. There are two right-hand polarized instability regions. One going from the origin to the point denoted by D, and the other from the C to B. The other two instability regions cover the gap between the origin and the point denoted by G. In Fig. 5c, we have raised the pump wave amplitude to $A = 0.1$, and we see that, except for the region between the points D and C, the whole right hand branch has been destabilized. In Fig. 5d we have raised the pump wave amplitude further to $A = 0.21$, and one can see that even the small stable region between D and C is now unstable. In other words, for a R-wave with $A \geq 0.21$ the branch of the dispersion relation above the pump wave frequency is completely destabilized. In this case the pump wave acts in the opposite direction than the left hand pump, i. e., it helps the destabilization of the this branch. For the same parameters of Fig. 5b, in Fig. 6a we show again the dispersion relation x vs. y, and concentrate on the gap between the origin and the point denoted by G in Fig. 5a. This region involves an r-instability which goes from the origin to the point $x = 0.1025$ and $y = 0.1$, and a l-instability going from this point to G. In Fig. 6b, the wave amplitude has been raised to $A = 0.8$. From this figure it follows that the point G is now closer to the origin, showing stabilization of the l-instability. In Fig. 6c, we have raised $A = 1.35$ in order to show that the whole region is now stable.

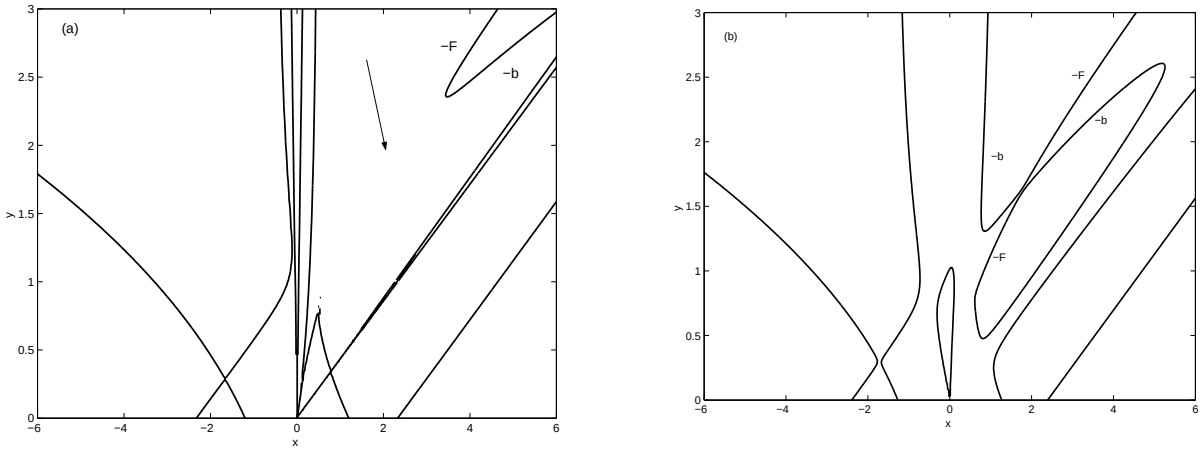

Figure 2. Same as Fig. 1, but $x_0 = 0.5$ for (a) $A = 0$, and (b) $A = 0.7$.

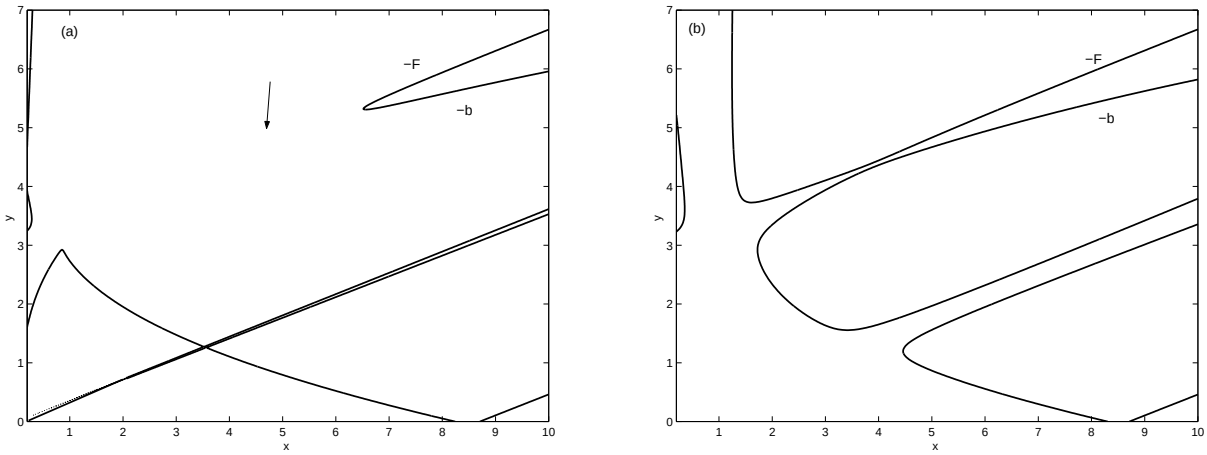

Figure 3. Nonlinear dispersion reltion, Eq. (3), x vs. y, for $\eta = 0.2$, $U = 2.8$, $\beta_i = 0.001$, $x_0 = 0.9$, for (a) $A = 0$, and (b) $A = 0.63$.

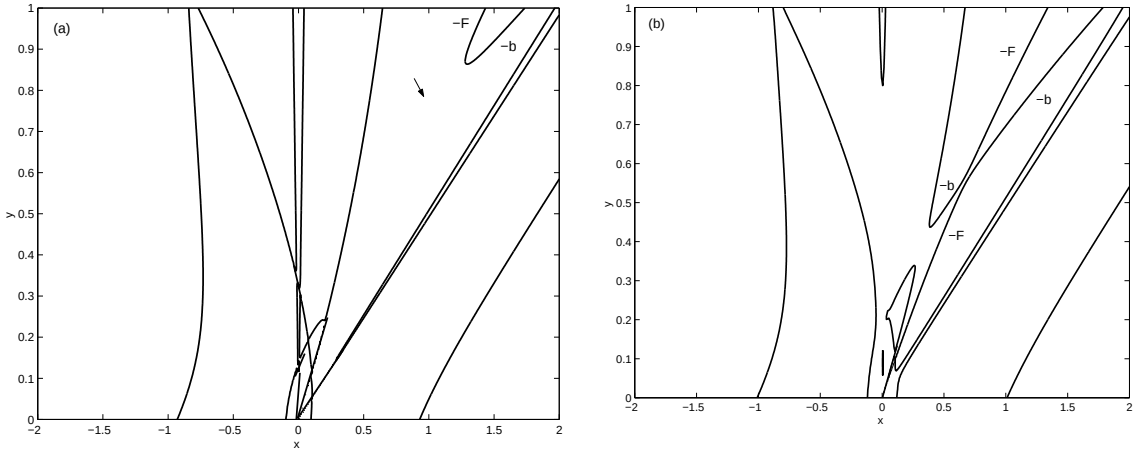

Figure 4. Same as Fig. 1, but for a right-hand polarized pump of frequency $x_0 = 0.1$ and $U = 2$, for (a) $A = 0$, and (b) $A = 0146$.

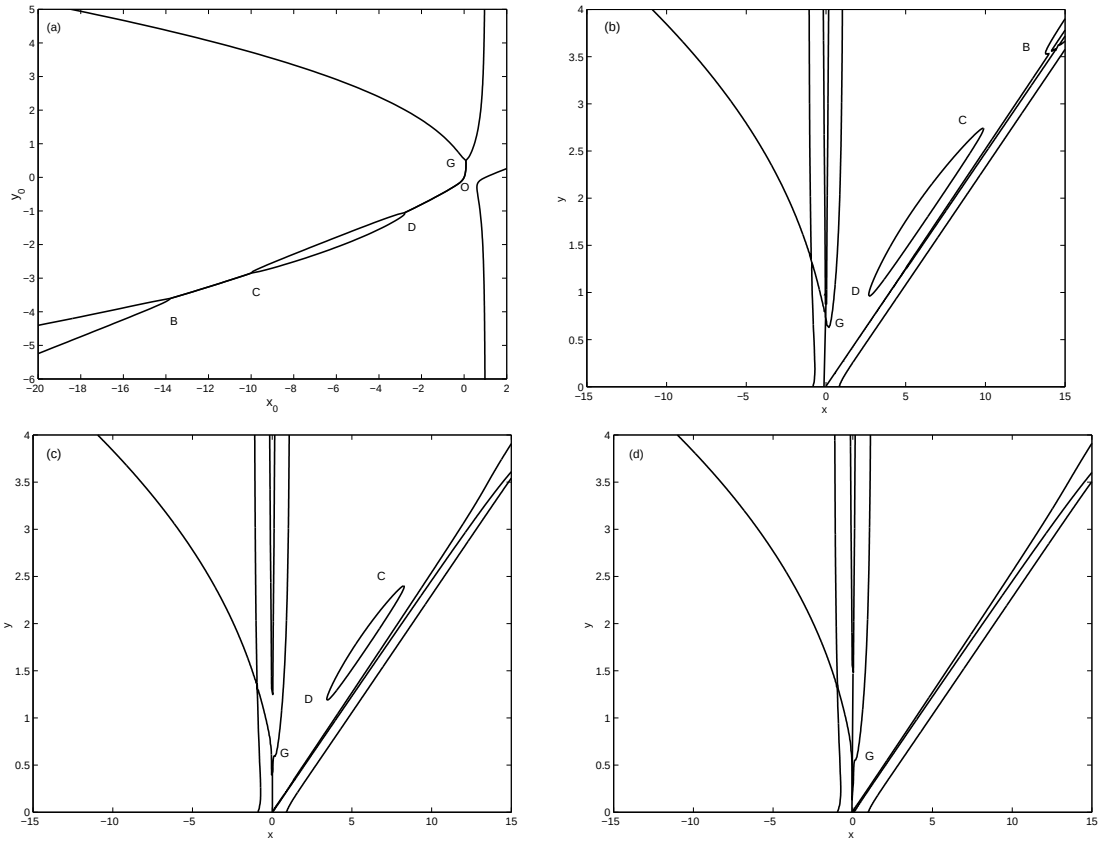

Figure 5. (a) Linear dispersion relation x_0 vs. y_0 for a right-hand polarized pump wave with $\eta = 0.2$ and $U = 4$. (b) Nonlinear dispersion relation x vs. y for a right-hand polarized pump wave of linearly unstable frequency $x_0 = 0.1025$, with $\eta = 0.2$, $\beta_i = 0.001$, $U = 4$ and $A = 0$, (c) $A = 0.1$, and (d) $A = 0.21$.

3.3 Electrostatic Instabilities in the presence of L-waves

We now study the ordinary ion-acoustic waves given by Eqs. (6-7) in the presence of an L-wave. In Fig. 7a we show the nonlinear dispersion relation for $x_0 = 0.3$ with corresponding $y_0 = 0.4033$ for $\beta_i = 0.01$ and $A = 0$, in this case there is no instability regions associated with the ion-acoustic waves. In Fig. 7b we have raised the L-wave amplitude to $A = 0.293$ and the arrow in the figure indicates how the phase velocities of the ordinary ion-sound waves approach each other. In Fig. 7c we have raised $A = 0.3$, the arrow in the figure shows it has appeared an instability region that correspond to an interaction between these sound waves. This instability is electrostatic in origin and does not correspond to parametric decays of the large amplitude wave, because it does not involve modes associated with the band waves. The free energy source of this instability is derived from the kinetic energy of the proton beam. In general we have found that this instability appears for L-wave amplitudes above a threshold amplitude.

4 Summary and Conclusions

By solving graphically the nonlinear dispersion relation Eq. (5) [30], we have shown the following properties of a system containing a finite amplitude circularly polarized wave propagating in a linearly unstable beam-plasma system. First, we assumed an L-wave and we showed that as the beam velocity increases the threshold A_t-value also increases. On the other hand, for fixed drift velocity, the threshold required to stabilize the linear r-instability decreases with increasing pump wave frequency. In Fig. 8. the results are extended to various values of β_i and L-wave frequencies for $U = 2.2$ and $U = 2.3$. As it follows from Fig. 8, A_t increases with increasing drift velocity, and decreases with increasing wave frequency for fixed drift velocity.

These results may have important applications. For example, [17] using hybrid simulations for a solar wind type plasma showed that the ion beam instability leads to a proton beam anisotropy $\Gamma_b = T_\perp/T_\| > 1$ [see Figs. 2a and 4a]. This result is consistent with previous similar studies for other space environments [3]. However, these results are in contradiction with the observations performed by [31] which show the opposite tendency, i. e., $\Gamma_b \leq 1$. One possible explanation for the discrepancy is the absence of large amplitude waves (see Figs. 2b-2c, and Fig. 3, and also Figs. 4b-4c, and Fig. 5).

Moreover, there seem to be contradictory observations from Helios [18] and Ulysses [32], concerning the proton/proton drift velocity. [18] found that more than 20% of the observations were apparently above the linear threshold for instability, while further away from the Sun, at 3 AU, [32] found that most of the events lie below the linear instability threshold. On the other hand, according to quasi linear

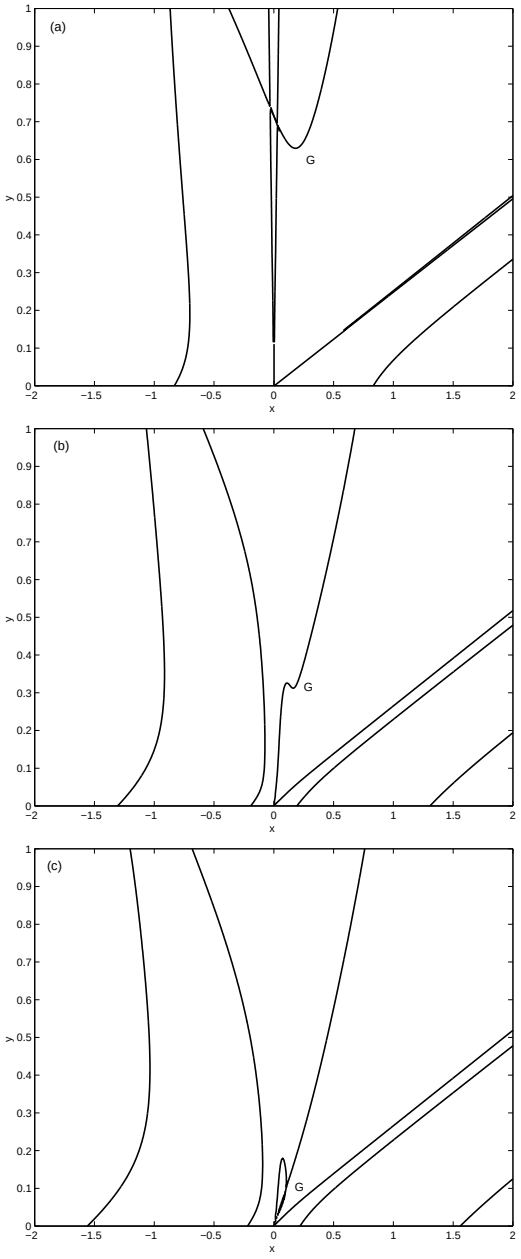

Figure 6. Same as Fig. 5b for (a) $A = 0$, (b) $A = 0.8$, and (c) $A = 1.35$.

linear theory [4] and simulation experiments [17], the instability must lead to a decrease of the drift velocity below the threshold value, and to an increase in the thermal anisotropy of the proton beam, i. e., $\Gamma_b > 1$. However, at least in the case of Helios, some of the observations of the drift velocity lie above the instability threshold, $2 \leq$U≤ 4. The persistence of these unstable distribution has been a problem awaiting resolution [17]. In addition proton beams do not show a clear increase in the thermal anisotropy, $\Gamma_b > 1$, [31]. If, however, large amplitude left-handed waves are present in the system, the threshold beam drift velocity for linear instability increases (relative to the threshold in the absence of large amplitude waves) rendering the system linearly stable [1].

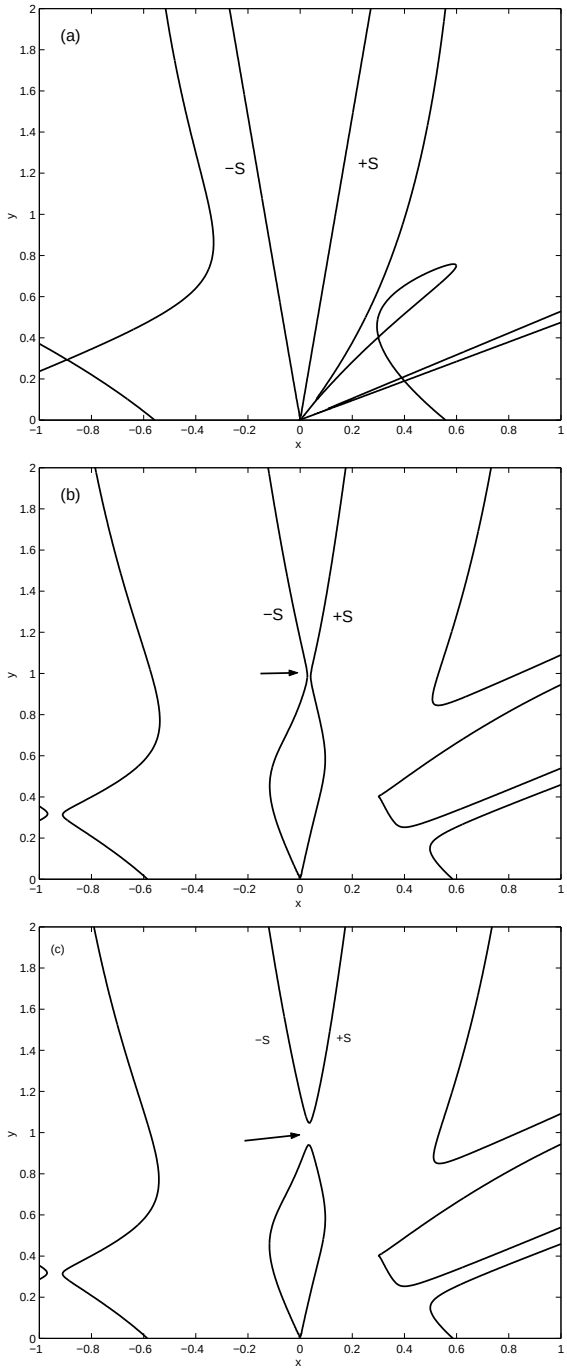

Figure 7. Dispersion Relation, Eq.(5), showing the ion acoustic waves ($-S$,$+S$) for $U = 2.0$, $\beta_i = 0.01$, $x_0 = 0.3$, $y_0 = 0.4033$, (a) $A = 0$, (b) $A = 0.293$, the arrow in the figure indicates that the phase velocities of the ordinary ion-sound waves approach each other. (c) $A = 0.3$, the arrow in the figure shows the instability region corresponding to the electrostatic instability.

Next, we studied the effect of an R-wave on l/r-linear beam-plasma instabilities. We considered the case when the frequency of the R-wave is in a region where the system is linearly stable, and second in a region where the system is linearly unstable [2]. We showed that the presence of the R-wave can stabilize the linear instability. This is illustrated in Fig. 4. In Table 2., these results are generalized for various frequencies and values of β_i. As it follows from Table 2,

TABLE 2. Threshold R-wave amplitude, A_t, for various pump wave frequencies, and β_i

η	U	x_0	y_0	β_i	A_t
0.2	2.0	0.001	0.00116	0.001	0.153
				0.01	0.151
				0.1	0.135
				1.0	0.100
		0.01	0.011581	0.001	0.151
				0.01	0.150
				0.1	0.134
				1.0	0.110
		0.1	0.112560	0.001	0.144
				0.01	0.142
				0.1	0.123
				1.0	0.100

A_t increases with decreasing β. This behavior is similar to the one encountered in the case of a L finite amplitude wave. On the other hand, the presence of the wave stabilizes the region between the pump wave frequency and O, and the region between O and G, for $A \geq A_t$ (see Fig. 6). In this case, the finite amplitude wave can be triggered by the linear instability itself, and if its amplitude can grow until $A = A_t$, the linear instability can be saturated by the same wave triggered by the instability.

Thus, we have shown that a finite amplitude L/R-wave can act as a saturation mechanism for r/l hand polarized instabilities. Another way of looking at these results is the following. Linear beam-plasma electromagnetic instabilities behave in a different way in the presence of a finite amplitude L/R wave. For example, in the linear theory and in the absence of a finite amplitude wave, in order to trigger the r-instability, the drift velocity of a proton beam with $\eta = 0.2$ moving in the direction of an external magnetic field, must have a drift velocity $U \geq 1.95$ [24, 33]. However, the presence of a finite amplitude polarized wave can stabilize the linear instability when the amplitude satisfies $A \geq A_t$. For the particular case when $U = 2.0$ with the other parameters like in Fig. 1, the system is completely stabilized in the presence of a L-wave with $A_t \simeq 0.16$ [1]. This result is shown in Fig. 9a. This means that in the presence of the L-wave with $A = 0.16$, a larger beam drift velocity is required to trigger the r-instability. In fact, in Fig. 9b we have increased from $U = 2.0$ to $U = 2.1$ in order to show that the instability has reappeared. Of course if $A \gg A_t$, a much larger drift velocity is required to trigger the instability.

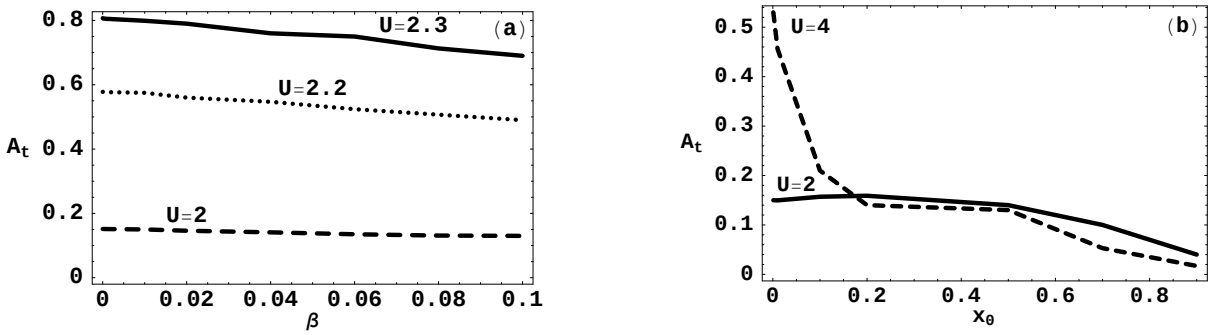

Figure 8. (a) Threshold L-wave amplitude, A_t, vs. β_i, for fixed $x_0 = 0.001$ and several U values: $U = 2.0$ (dashed line), $U = 2.2$ (dotted line), and $U = 2.3$ (full line). (b) Threshold L-wave amplitude, A_t, vs. frequency, x_0, for fixed $\beta_i = 0.01$, and $U = 2$ (full line), and threshold R-wave amplitude for complete destabilization of the r-instability for the same β_i but $U = 4$ (dashed line).

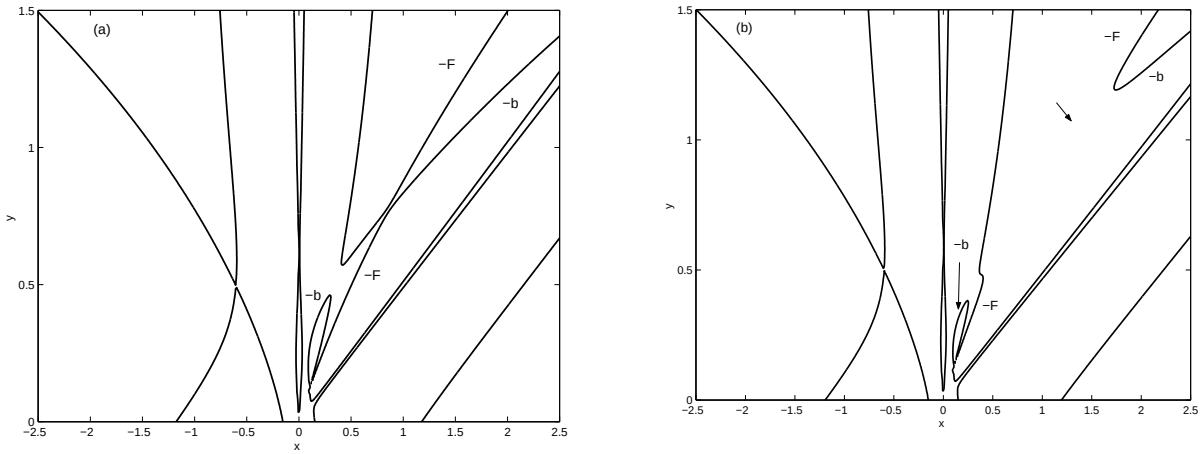

Figure 9. Same as Fig. 1, but for (a) $U = 2.0$ and $A_t = 0.16$, showing the stabilization of the linear right-hand instability, and (b) $U = 2.1$ and $A_t = 0.16$, showing the destabilization of the linear instability.

Finally, in Fig. 7. we have shown the presence of an L-wave can trigger electrostatic instabilities. These instabilities occur when the phase velocities of two ion-acoustic waves become equal.

Acknowledgments

This work has been partially supported by FONDECYT grants 1020152 and 7020152. One of us (J. H.) thanks MECESUP for a doctoral fellowship.

References

[1] L. Gomberoff, J.Geophys.Res. **108** A6, 1261, doi: 10.1029/2003JA009387(2003).

[2] L. Gomberoff, J. Hoyos, and A. L. Brinca, J. Geophys. Res. **108**, A12,1472, doi:10.1029/2002JA00576(2003).

[3] S. Gary, Space Sci. Rev. **56**, 573 (1991).

[4] E. Marsch, *Kinetic Theory of the Solar wind Plasma in The Physics of the inner Heliosphere*, edited by E. Marsch and R.S. Schwenn. p.539, Pergamon, N. Y. (1991).

[5] M.M. Hoppe, C. T. Russell, L. A. Frank, T. E. Eastman, and E. W. Greenstadt, J. Geophys. Res. **86**, 4471 (1981).

[6] M.M. Hoppe, C. T Russell, T. E. Eastmann, and L. A. Frank, J. Geophys. Res. **87**, 643 (1982).

[7] M.D. Leubner, and A. Viñas, J. Geophys. Res. **91**, 13366 (1986).

[8] R.M.O. Galvão, G. Gnavi, F. T. Gratton, and L. Gomberoff, Phys Rev. E. **54**, 4112 (1996).

[9] J.V. Hollweg, R. Esser, and V. Jayanti, J. Geophys. Res. **98**, 3491 (1993).

[10] V. Jayanti and J. Hollweg, J. Geophys. Res. **99**, A12, 23449, doi: 10.129/94JA02370 (1994).

[11] L. Gomberoff, F. T. Gratton, and G. Gnavi, J. Geophys. Res. **99**, 14, 717 (1994).

[12] B.A. Inhester, B. A., J. Geophys.Res. **95**, 10, 525 (1990).

[13] V.J. Vasquez, J.Geophys. Res. **100**, 1779 (1995).

[14] L. Gomberoff, J. Geophys. Res. **105**, 10, 509 (2000).

[15] L. Gomberoff, K. Gomberoff, and A. L. Brinca, J. Geophys. Res. **106**, 18, 713 (2001).

[16] L. Gomberoff, K. Gomberoff, and A. L. Brinca, J.Geophys. Res. **107**, 1123, doi:10.1029/2001JA000265 (2002).

[17] W. Daughton, S. P. Gary, and Dan Winske, J. Geophys. Res. **104**, 4657 (1999).

[18] E. Marsch, and S. Livi, J. Geophys. Res. **92**, 7263 (1987).

[19] J. A. Araneda, J. A., and L. Gomberoff, J. Geophys. Res. **109**, A01106,doi:10.1029/2003010189 (2004).

[20] V. Jayanti, and J. V. Hollweg, J. Geophys. Res. **98**, 13, 247 (1994a).

[21] L. Gomberoff, L., IEEE Transactions on Plasma Science, **20**, 843 (1992).

[22] L. Gomberoff, and R. Elgueta, J. Geophys. Res. **96**, 9801 (1991).

[23] L. Gomberoff, and R. Hernández, J. Geophys. Res. **97**, A8, 12, 113-12, 116 (1992).

[24] L. Gomberoff, and H. F. Astudillo, Planet. Space Sci. **46**, 1683 (1998).

[25] L. Gomberoff, F. T. Gratton, and G. Gnavi, J. Geophys. Res. **100**, 1871 (1995).

[26] L. Gomberoff, F. T. Gratton, and G. Gnavi, J. Geophys. Res. **99**, 14, 717 (1994).

[27] L. Gomberoff, and R. Neira., J. Geophys. Res. **88**, 2170 (1983).

[28] S. R. Cranmer, Space Sci. Rev. **101**, 229 (2002).

[29] J. V. Hollweg, and P. A. Isenberg, J. Geophys. Res. **107**, 1147, doi:10.1029/2001JA000270(2002).

[30] M. Longtin, and B. U. O. Sonnerup, J. Geophys. Res. **91**, 6816 (1986).

[31] W. C. Feldman, J. T. Gosling, D. J. McMcComas, and J. L. Phillips, J. Geophys. Res. **98**, 5593 (1993).

[32] B. E. Goldstein, N. Neugebauer, L. D. Zhang, and S. P. Gary, Geophys. Res. Lett. **27**, 53 (2000).

[33] K. Gomberoff, L. Gomberoff, and H. F. Astudillo, J. Plasma Phys. **64**, 75 (2000).